

Banner appropriate to article type will appear here in typeset article

Prediction of flow and elastic stresses in a viscoelastic turbulent channel flow using convolutional neural networks

Arivazhagan G. Balasubramanian^{1,2}†, Ricardo Vinuesa^{1,2} and Outi Tammisola^{1,2}

¹FLOW, Engineering Mechanics, KTH Royal Institute of Technology, Stockholm, Sweden

²Swedish e-Science Research Centre (SeRC), Stockholm, Sweden

(Received xx; revised xx; accepted xx)

Neural-network models have been employed to predict the instantaneous flow close to the wall in a viscoelastic turbulent channel flow. The numerical simulation data at the wall is utilized to predict the instantaneous velocity fluctuations and polymeric-stress fluctuations at three different wall-normal positions. Apart from predicting the velocity fluctuations well in a hibernating flow, the neural-network models are also shown to predict the polymeric shear stress and the trace of the polymeric stresses at a given wall-normal location with reasonably good accuracy. These non-intrusive sensing models can be integrated in an experimental setting to construct the polymeric-stress field in turbulent flows, which otherwise may not be directly quantifiable in experimental measurements.

Key words: turbulence simulation, viscoelastic turbulent channel flow, fully convolutional networks

1. Introduction

Viscoelastic fluids are widely used in industrial processes, and an understanding of complex-fluid behaviour becomes crucial for enterprises working with non-Newtonian flows. Further, in real-world scenarios, turbulent flows predominate, exhibiting chaotic and multi-scale dynamics. The turbulent flows of purely viscoelastic fluids have important technological implications due to increased mixing efficiencies at low Reynolds numbers and have also piqued the interest in drag-reduction and flow control communities at high Reynolds numbers. The addition of a tiny amount of polymer (parts per million) has proven efficient in reducing friction drag in pipe flows (Virk 1971), leading to substantial energy savings in fluid-transport applications. Drag reduction by polymers (elasticity) is related to their ability to modify coherent structures in wall-bounded turbulence (Dubief *et al.* 2004, 2005). Elasticity influences the turbulent cycle in two ways: by attenuating near-wall vortices, but at the same time increasing the streamwise kinetic energy of the near-wall streaks. Additionally, Xi & Graham (2010, 2012) suggested that the turbulent flow is characterized by an alternating

† Email address for correspondence: argb@mech.kth.se

sequence of active and hibernating phases. These phases are distinguished by flow structures exhibiting strong vortices and wavy streaks during the active phase, and weak streamwise vortices during the hibernation phase, with viscoelastic flows characterized by increased hibernation intervals. Additional insights into the influence of polymer additives on drag reduction are detailed in [Xi \(2019\)](#).

Identifying such effects of elasticity sparked an interest to detect and understand drag-reducing behaviour in the presence of both elasticity and plasticity in the fluid. [Le Clairche et al. \(2020\)](#) analysed the simulation data of [Rosti et al. \(2018\)](#) using high-order dynamic mode decomposition, and compared the modes in complex fluids (non-Newtonian fluids) with those in Newtonian fluids. Their results indicated that elasticity and plasticity of the complex fluids have similar effects on the coherent structures; in both cases, the flow is dominated by long streaks disrupted by rapid, localised perturbations. On the other hand, the Newtonian flow displays short streaks and more chaotic dynamics. [Izbassarov et al. \(2021\)](#) found that the largest amount of drag reduction is achieved with a combination of finite elasticity and plasticity, and while the highly plastic flow (high Bingham numbers) relaminarizes, elasticity affects the relaminarization in a complex and non-monotonic fashion.

However, when it comes to canonical (and practical) flows of interest, direct numerical simulations (DNSs) of viscoelastic (and/or elasto-viscoplastic) flow face challenges due to substantial computational costs associated with capturing the diverse physical mechanisms driving the flow. On the other hand, experimental investigations of drag reduction in viscoelastic flows encounter limitations stemming from near-wall measurements and the capabilities of experimental techniques to accurately quantify the flow, without perturbing it. While a complete description of viscoelastic turbulence would require characterization of both velocity and polymeric stresses. However accessing such polymer deformation directly from experimental measurements remains a challenging goal.

In recent years, machine-learning methods have provided a significant advance over prior methodologies in various applications within the field of fluid mechanics ([Vinuesa 2024](#)). Specifically in the domain of viscoelastic flows, researchers have explored the predictability of polymer stress components from velocity gradient using neural networks ([Nagamachi & Tsukahara 2019](#)). Towards estimation of fluid flow, neural-network models have demonstrated excellent capabilities in predicting the instantaneous state of the Newtonian turbulent flow using quantities measured at the wall ([Guastoni et al. 2021](#)). Hence in the present study, the idea of non-intrusive sensing has been applied to viscoelastic turbulent channel flow to predict the velocity fluctuations and polymeric stress components near the wall using the quantities measured at the wall. To this end, the convolutional-neural-network (CNN) models are employed to predict the two-dimensional velocity fluctuations and polymeric-stress fluctuation fields at different wall-normal distances. The present work highlights the capability of a data-driven approach to model turbulence in complex-fluids flows. In addition, the developed non-intrusive sensing models will also find useful applications in experimental settings and in closed-loop control of wall-bounded turbulence in viscoelastic flows.

2. Methodology

2.1. Dataset

The dataset for training and evaluation of the network model is obtained through a direct numerical simulation of turbulent channel flow of viscoelastic fluid at a Reynolds number based on the bulk velocity of $Re = U_b h / \nu = 2800$ (where the bulk velocity U_b corresponds to the average value of the mean velocity in the whole domain, h is the channel half-height and $\nu (= \mu_0 / \rho)$ denotes the kinematic viscosity of the fluid, with ρ and μ_0 being the density and

total viscosity of the fluid, respectively), which corresponds to a friction Reynolds number $Re_\tau = 180$ (where Re_τ is defined in terms of h and friction velocity u_τ) for a Newtonian fluid. In this study, the turbulent channel flow simulations are performed at a Weissenberg number $Wi = 8$, (where $Wi = \lambda U_b/h$, with λ corresponding to the relaxation time of the polymeric stresses and Wi quantifies the elastic forces with respect to the viscous forces, thereby quantifying the degree of anisotropy in the flow). The ratio of polymeric viscosity (μ_p) to the total viscosity (μ_0), which is denoted by α , is set to 0.1, indicating that we consider a dilute polymer concentration of the viscoelastic fluid. The polymeric-stress tensor (τ_p) is modelled using the finite extensible nonlinear elastic-Peterlin (FENE-P) model, with maximum polymer extensibility $L = 60$. The difficulties associated with proper rheological characterization of real fluids by adequate constitutive equations is an important area of research on its own and rather, we assume that the adopted model adequately describes the intended fluid properties. Furthermore, to circumvent the high Weissenberg number problem, log-conformation approach (Fattal & Kupferman 2004) is utilized to ensure the positive-definiteness of the conformation tensor. Here, the conformation tensor provides a macroscopic view of the polymer deformation.

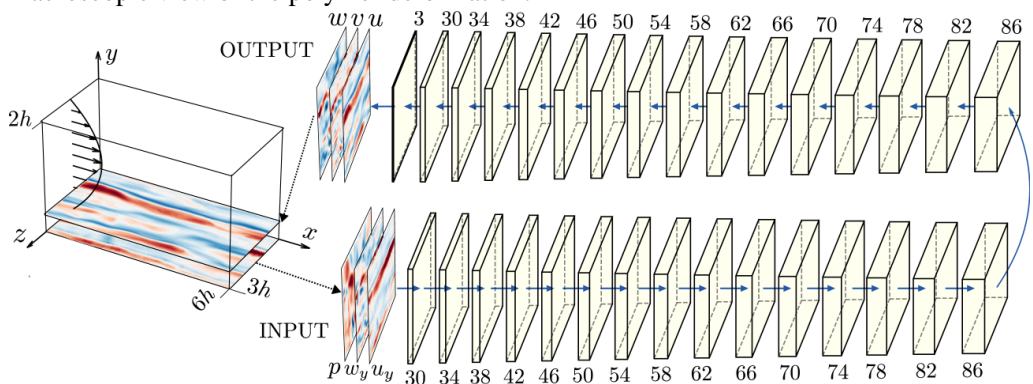


Figure 1: Typical workflow representation of V-prediction using fully-convolutional network (FCN) model. (Left) Computational domain for the channel flow and (right) FCN model with the corresponding number of kernels in each hidden layer is indicated.

The viscoelastic turbulent channel flow is simulated using a finite-difference-based in-house code on a computational domain of size $6h \times 2h \times 3h$ in the streamwise (x), wall-normal (y) and spanwise directions (z), respectively as shown in figure 1. The readers are referred to Izbassarov *et al.* (2021) for a complete description of the viscoelastic turbulent channel simulation employed in this study. The computational domain is uniformly discretized using $1728 \times 576 \times 864$ grid points along x, y and z , respectively. The spatial resolution of $\Delta x^+ = \Delta y^+ = \Delta z^+ < 0.6$ is chosen to fully resolve the turbulent scales in the viscoelastic turbulent flow (Rosti *et al.* 2018). Here, the superscript ‘+’ denotes the scaling in terms of friction velocity $u_\tau (= \sqrt{\tau_w/\rho}$, where τ_w corresponds to the wall-shear stress) as the velocity scale and viscous length $\ell^* (= \nu/u_\tau)$ as the length scale. Note that the value of u_τ obtained with $Wi = 8$ is lower than that in the Newtonian case ($u_\tau \approx 180/Re_b$; since, $Re_\tau, Wi=0 \approx 180$) due to skin-friction reduction. Variation of the averaged wall-shear rate ($\langle \langle U_y \rangle_{x,z} |_{\text{wall}} \rangle$) obtained with $Wi = 8$ is compared against the Newtonian case ($Wi = 0$) in figure 2. Here, U_y corresponds to the wall-normal derivative of the streamwise velocity and $\langle \cdot \rangle_{x,z}$ denotes the spatial averaging in x and z directions in the channel. The Reynolds decomposition of an instantaneous field U is denoted as $\langle U \rangle_{x,z,t} + u$, with u identifying the fluctuations. From figure 2, identifying the hibernation intervals (regions with low wall-shear stress) using area-averaged wall-shear

rate as performed in Xi & Graham (2010) with a threshold corresponding to 10% of the mean shear-rate, we observe the presence of such low-drag events at $Wi = 8$, where polymer stretching is weakest. Note that the choice of threshold is arbitrary here and a definitive choice of the threshold value is absent in the literature. Effectively, for the considered viscoelastic turbulent flow at $Wi = 8$, we observe a drag reduction of roughly 20% for the set of considered parameters in this study. From figure 2, it is evident that the wall-fields (which are provided as inputs to FCN, see figure 1, §2.2) are significantly varying from the statistical mean for a considerable fraction of the total time. Thus, in this work we aim to build a neural-network model that can predict viscoelastic turbulence quantities of interest, not only in the mean-flow but also in extreme wall-shear events with particular interest in hibernation intervals.

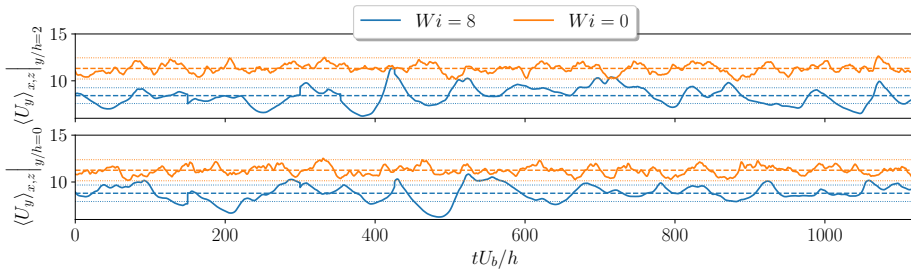


Figure 2: Temporal variation of wall-shear-rate in a viscoelastic channel flow corresponding to $Wi = 8$ and Newtonian channel flow ($Wi = 0$) at (top) $y/h = 2$ and (bottom) $y/h = 0$. The dashed lines indicate the temporal mean and the dotted lines indicate the 10% deviation from the temporal mean.

To this end, a database consisting of instantaneous fluctuation fields of wall-shear-stress components, wall-pressure fluctuation, two-dimensional velocity-fluctuation and polymeric-stress-fluctuation fields are obtained at different wall-normal locations, $y^+ \approx 13.6, 26.7$ and 44.2 ($y/h \approx 0.09, 0.17$ and 0.28 , respectively). Note that these wall-normal locations correspond respectively to $y^+ = 15, 30$ and 50 for a Newtonian turbulent channel flow and hence, for simplicity we refer to these locations as $y^+ \approx 15, 30$ and 50 , respectively in this study. The simulations are run for $\sim 120h/u_\tau$ time-units and a total of 40,600 samples is obtained with a sampling period of $\Delta t_s^+ \approx 1$ for training the network model. The sampled instantaneous two-dimensional fields are down-sampled to a resolution of 432×432 in x and z , respectively. The fields at both the walls are utilized in this study, and they are split into training and validation set with a ratio of 4 to 1. The network models are evaluated with the samples in the test dataset which consists of 10,000 samples. The samples in the test dataset are chosen from a time-interval (in the sampled time series) that corresponds to at least 60 flow-through times apart from the samples in the training dataset to ensure minimal autocorrelation between the samples in training and test dataset. The number of samples in the test dataset is chosen to obtain convergence of second-order turbulence statistics.

2.2. Neural-network model

In this work, a fully convolutional neural network (FCN) similar to the one proposed by Guastoni *et al.* (2021) is used, with increased hidden layers (see figure 1) to obtain a more complex combination of abstract turbulent features identified by the kernels in the network. Here, we utilize an existing architecture, acknowledging that further enhancements could be achieved with newer architectures that require extensive datasets. Our focus is on proposing a methodology for viscoelastic stress predictions in turbulent flows aimed towards experimental applications and in establishing baseline performance using current convolutional architectures. The considered FCN consists of 30 hidden layers with a total number of trainable parameters amounting to 985,105. The convolution operations are

followed by a batch normalization and a rectified-linear-unit (ReLU) activation function. The inputs to the network are normalized using respective mean and standard deviation of the fields from the training dataset and the outputs are normalized using the corresponding standard deviation values. The choice of loss function in the network is the mean-squared error (MSE) between the instantaneous predicted and DNS fields, which helps the network to learn the large-scale features first and then progressively optimize the trainable parameters to minimize the errors at finer scales (Xu *et al.* 2019).

In this study, three types of predictions have been undertaken to highlight the capability of FCN models to reconstruct the near-wall visco-elastic turbulence fields. In V-predictions (indicating velocity predictions), the streamwise wall-shear, spanwise wall-shear and pressure field at the wall are utilised to predict the streamwise, spanwise and wall-normal velocity-fluctuations. This allows us to assess whether velocity fields can also be predicted in a viscoelastic turbulence exhibiting periods of hibernation. The performance of neural-network models in predicting the fluctuations of polymeric-shear stress ($\tau_{p,xy}$) and fluctuations of trace of polymer stress ($\text{tr}(\tau_p)$) at a given wall-normal location using the true velocity-fluctuation fields at the same location, and they are denoted as E-predictions (signifying prediction of elastic stress quantities of interest). Finally in V-E-predictions, the FCN model is used to predict the fluctuations of polymeric-shear stress and diagonal components of polymer-stress tensor at a target wall-normal distance directly from wall inputs, with auxiliary predictions of corresponding velocity-fluctuations at the considered wall-normal location. †

The network performance is evaluated from a statistical point of view in terms of the relative-error in predicting the corresponding root-mean-squared (RMS) quantities between the true (DNS) fields from test dataset and predicted fields from FCN (indicated by E_{RMS}). The mean-absolute error between the predictions and DNS fields (denoted by MAE) is also reported for different types of predictions. Note that the performance metrics reported in this study are obtained from the mean of at least three different network models to include the effects of stochasticity introduced by the random initialization of kernel weights in FCN and random sampling of mini-batches during the training process. The instantaneous correlation coefficient between the predicted and DNS fields, averaged over the samples in the test dataset, is also highlighted. To evaluate the distribution of energy in different length scales, a comparison of the pre-multiplied two-dimensional (2D) power-spectral density (PSD) $k_z k_x \phi_{ij}(\lambda_x^+, \lambda_z^+)$ between DNS fields and the predictions is performed. Here, ϕ_{ij} is the power-spectral density obtained for the quantity 'ij' and k_x, k_z respectively denote the wavenumbers in streamwise and spanwise directions with the corresponding wavelengths in viscous units denoted by λ_x^+ and λ_z^+ .

3. Results

3.1. V-predictions

A qualitative prediction field for V-predictions is shown in figure 3 (corresponding to an instant in the test dataset where the input wall-shear rate is higher than the mean wall-shear rate). We observe the predicted velocity fields to be visually well correlated with the DNS fields at different target wall-normal locations. The linear correlation coefficient between the predicted and true streamwise-velocity fluctuation field exceeded 99% for predictions at $y^+ \approx 15$, and gradually declining but remaining above 80% at $y^+ \approx 50$. The RMS quantities of the streamwise velocity-fluctuation fields at $y^+ \approx 15, 30, 50$ are predicted with less than ($E_{\text{RMS}} <$) 3%, 6% and 15% error, respectively. With an increasing

† The auxiliary predictions of velocity-fluctuations at a wall-normal location is utilized in V-E predictions to obtain an increase in the accuracy of prediction of polymeric stress quantities.

separation distance (wall-normal distance between the wall fields and the target velocity-fluctuation fields), the fields are less-correlated and thereby the performance of the network also decreases. Because of this, the RMS-normalized mean-absolute errors in the predicted streamwise-velocity fluctuations are 0.14, 0.29 and 0.47 at $y^+ \approx 15, 30, 50$, respectively (see also figure 4).

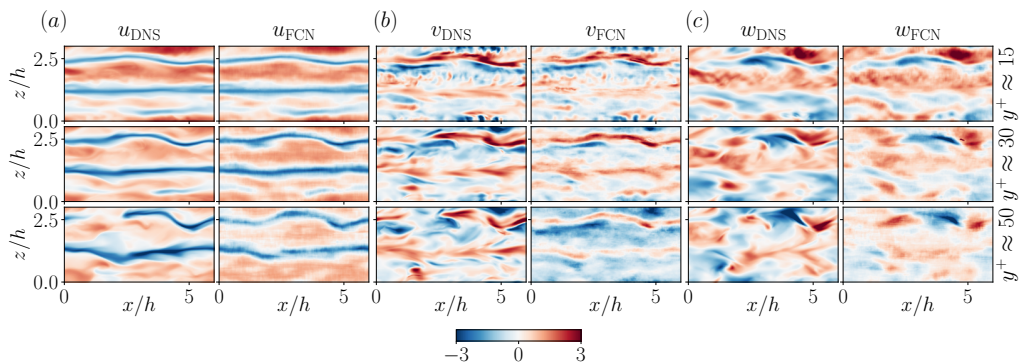


Figure 3: Comparison of the instantaneous velocity-fluctuation fields in the (a) streamwise, (b) wall-normal and (c) spanwise direction, at different y^+ . In (a – c): (left) corresponds to the DNS field and (right) shows the corresponding V-predictions from FCN. The fields are scaled with the corresponding RMS values.

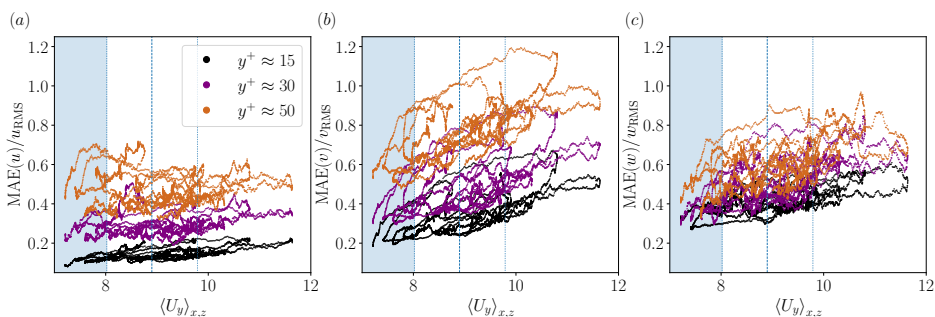


Figure 4: Variation of the RMS-normalized mean-absolute errors of (a) streamwise, (b) wall-normal and (c) spanwise velocity components in V-predictions at different wall-normal locations with respect to the wall-shear rate. The markers correspond to the mean absolute error in the instantaneous sample in the test dataset. Shaded region corresponds to the hibernation interval identified with 90% of $\langle U_y \rangle_{x,z,t}$.

The MAE in the wall-normal and spanwise fluctuation fields remained below 0.025 in the different target wall-normal locations considered in the study. However, the E_{RMS} values in the wall-normal and spanwise velocity fluctuations are at least twice as large as those obtained in the RMS prediction of the streamwise component at the respective wall-normal locations. This is due to the influence of the polymers, which reduce turbulence by opposing the downwash and upwash flows generated by near-wall vortices (Dubief *et al.* 2004, 2005). Due to the absence of polymeric-stress information in the inputs to the network model for V-predictions, an accurate representation of the turbulence statistics in the spanwise and wall-normal fluctuation components becomes challenging.

It should be emphasized that the network model is explicitly optimized for predicting instantaneous fields rather than reproducing the turbulence statistics. This emphasis is rooted in the motivation for non-intrusive sensing in an experimental setting, aimed at understanding the near-wall dynamics of viscoelastic turbulent channel flow. In addition, optimizing network models to accurately replicate turbulence statistics obtained from DNS could lead the model

to learn the mean-flow behavior with a lower E_{RMS} . This may also entail a compromise, as predictions during hibernating intervals could potentially become less accurate.

When assessing the accuracy of the instantaneous predictions based on mean-absolute errors, as illustrated in figure 4, it becomes apparent that the MAE (in each test sample) varies with wall-shear rate for different target wall-normal locations. Specifically, in instances of low-wall-shear-rate, the absolute errors are notably lower, and increase with wall-shear rate. This is due to the fact that low-drag events typically exhibit reduced fluctuation intensity and it increases with wall-shear rate, leading to increased concentration of energy in small-scale features. Consequently, the network encounters relative difficulty in accurately predicting these small-scale features, resulting in higher prediction errors at large wall-shear-rate inputs. It is worth noting that the variation of MAE (in each test sample) with wall-shear rate stems from the selection of the loss function utilized in the network. Nevertheless, the obtained network model exhibits superior predictive performance in capturing velocity-fluctuation fields during low-wall-shear rate events. This observation underscores the potential utility of such models in obtaining sufficiently accurate velocity fluctuations in an experimental setting, more particularly for studying hibernation events in detail.

3.2. E -predictions, V - E -predictions

A sample predicted field (corresponding to the same wall inputs as in figure 3) for E -predictions and V - E -predictions is shown in figure 5. Overall, the large-scale features in the polymer-stress quantities of interest are visually well-corresponding. For E -predictions, where polymeric stresses are predicted from DNS velocity fields at the same location there is no separation distance between the input and target fields and the linear correlation coefficient between the predicted and DNS polymer-shear stress, as well as with the trace of the polymer stress remained more than 90% for the different target wall-normal positions. Moreover, E_{RMS} remained below 15% for E -predictions of $\tau_{p,xy}$ and $\text{tr}(\tau_p)$ at different target y^+ .

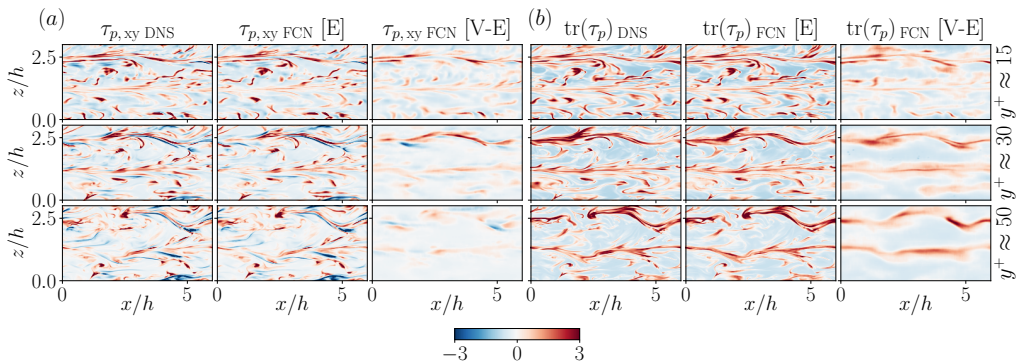


Figure 5: A sample fluctuation field corresponding to (a) polymer-shear-stress and (b) trace of the polymer-stress, at different-wall normal locations. In (a - b): (left) corresponds to DNS field, (middle) shows the E -predictions and (right) corresponds to V - E -predictions from FCN. The fields are scaled with the respective RMS values.

Note that in V - E -predictions the polymeric stresses are predicted directly from the wall inputs, without having access to the true velocity fields at the wall-normal location where those stresses are predicted. Instead, predicted auxiliary velocity fields at that location (together with wall inputs) are used to predict the polymeric stress fields. The obtained errors of around 40% indicate that a small error in predicting velocity-fluctuation fields significantly impacts the errors in predicting the polymeric-stress fields, indicating that the auxiliary velocity fluctuation fields in V - E -predictions lack certain information that is connected to the polymeric activity in the small wavelengths. Nevertheless, the large-scale

structures in the predicted polymeric-stress fields for V-E-predictions exhibit a qualitative agreement with the reference, as observed in figure 5.

Examining the accuracy of instantaneous predictions based on mean-absolute errors, as depicted in figure 6 for E-predictions and V-E-predictions, reveals a similar trend in MAE (in each test sample) with respect to wall-shear rate as observed in V-predictions. Overall, the absolute errors increase with wall-shear rate. Further, the magnitude of such absolute errors in the field is nearly doubled for V-E-predictions (figure 6*b, d*) compared to E-predictions (figure 6*a, c*). Moreover, the MAE in predicting polymer-stress quantities of interest remains relatively constant across various target wall-normal positions with respect to the corresponding RMS quantities for both E-predictions and V-E-predictions.

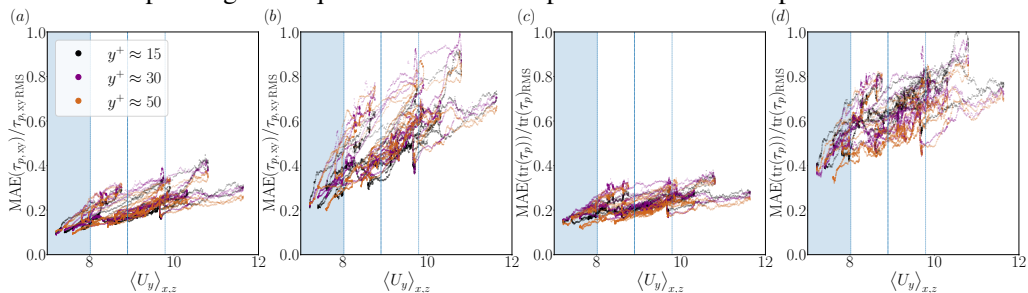


Figure 6: Variation of the RMS-normalized mean-absolute errors of polymer-shear stress in (a) E-predictions, (b) V-E-predictions and trace of polymer stress in (c) E-predictions and (d) V-E-predictions with respect to the wall-shear rate. The markers corresponds to the mean absolute error in the instantaneous sample in the test dataset. Shaded regions correspond to the identified hibernation interval with 90% of $\langle U_y \rangle_{x,z,t}$.

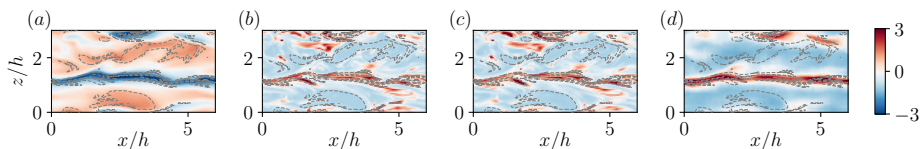


Figure 7: Comparison of RMS-scaled (a) streamwise velocity fluctuation field with (b) $tr(\tau_p)$ from test dataset at $y^+ \approx 50$. The corresponding (c) E-prediction and (d) V-E-prediction are shown. Strong anti-correlation zones are contoured.

The RMS of the trace of the polymer stress decreases as we move away from the wall for the considered y^+ locations and consequently the absolute errors in predicting $tr(\tau_p)$ decrease as the wall-normal distance increases. One plausible explanation for this phenomenon lies in the increased presence of energetic large-scale structures in the diagonal components of polymer stress tensor with respect to the wall-normal distance (see figure 8*b*). Further, the trace of the polymer stress exhibits an increasing anti-correlation with the streamwise velocity fluctuation as the wall-normal position increases as observed from figure 7, which is related to the polymers extracting turbulent kinetic energy (Dubief *et al.* 2005).

3.3. Power-spectral density

The distribution of energy in the predicted and DNS data across different scales are compared through the spectral analysis as illustrated in figure 8*a*. The results show that the neural-network models successfully reproduce the energy content in the streamwise velocity component (denoted by ϕ_{uu}) at different wavelengths. However, for the wall-normal velocity fluctuations (ϕ_{vv}) and spanwise velocity fluctuations (ϕ_{ww}), the network models exhibit limitations in reconstructing energy at the smallest wavelengths and specifically such errors in the smallest scales increase with increasing target wall-normal position.

The power-spectral density obtained for the polymeric-shear stress (denoted by $\phi_{\tau_p, xy} \tau_{p, xy}$) and the trace of polymer stress ($\phi_{\text{tr}(\tau_p) \text{tr}(\tau_p)}$) are depicted in figure 8b for different wall-normal positions. We observe that the energetic structures correspond to wavelengths that are almost one order of magnitude smaller than those observed in the velocity fluctuations (refer to figure 8a). This reveals that the polymer activity is predominantly concentrated in small-scale structures compared to the flow scales. Consequently, this suggests that the employed neural network model needs to reconstruct fine-scale polymer stress fields from coarse energy-containing features in the velocity fluctuations.

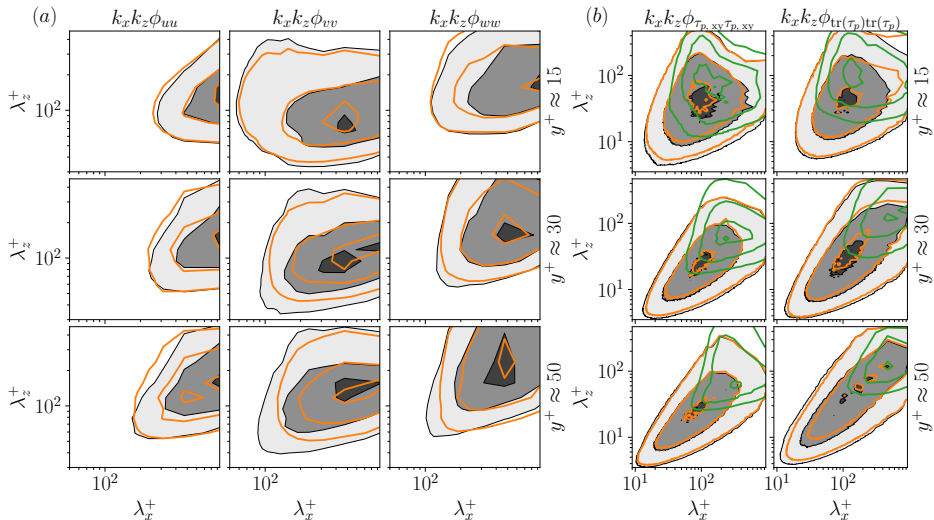


Figure 8: Pre-multiplied two-dimensional power-spectral densities of (a, left) the streamwise, (a, center) wall-normal, (a, right) spanwise velocity components and (b, left) polymer shear-stress, (b, right) trace of polymer stress at (top) $y^+ \approx 15$, (middle) $y^+ \approx 30$ and (bottom) $y^+ \approx 50$. The contour levels contain 10%, 50% and 80% of the maximum power-spectral density. Shaded contours refer to DNS data, while contour lines correspond to (a) V-predictions, (b, orange) E-predictions and (b, green) V-E-predictions.

For the E-predictions shown in figure 8b, we observe the ability of the model to reconstruct the features containing energy at different wavelengths more accurately with minimal errors observed in the smallest scales. However in the case of V-E-predictions, where the wall inputs to the network feature large-scale energy-containing features (not shown here), the performance of the network is reduced in reconstructing the energy distribution of features at smaller scales, and rather the model tends to predict the large-scale features in the polymer-stress fields.

4. Conclusions

The present work highlights the capability of a data-driven approach to perform non-intrusive sensing in viscoelastic turbulent flows. Here we demonstrate the ability of CNN-based models to accurately reconstruct the velocity fluctuations in viscoelastic turbulence close the wall, utilizing the two wall-shear fluctuation components and the wall-pressure fluctuations as inputs. Additionally, the network models successfully reproduce the polymeric-stress fluctuation fields from the DNS velocity-fluctuation fields. Moreover, the feasibility of these network models to extract polymer stress fluctuation fields of interest solely from wall input fluctuations and predicted velocity-fluctuations is explored. Overall, the network

effectively reconstructs the large-scale features of the polymer-stress fields using wall inputs and predicted velocity fields. Furthermore, the developed models exhibit enhanced accuracy in predicting quantities of interest during the hibernation intervals, facilitating a deeper understanding of the underlying physics during low-drag events when the model is deployed in a practical application. These non-intrusive-sensing models hold valuable applications in experimental settings (Vinuesa *et al.* 2023), enabling the construction of polymeric stresses in turbulent flows from velocity fields or wall-inputs, which otherwise would be challenging or impossible to quantify experimentally.

Acknowledgements. The authors acknowledge the National Academic Infrastructure for Supercomputing in Sweden (NAISS) for providing the computational resources to carry out the numerical simulations and training of convolutional network models.

Funding. This work is supported by the funding provided by the European Research Council grant no. "2021-StG-852529, MUCUS" and the Swedish Research Council through grant No 2021-04820. RV acknowledges the ERC grant no. "2021-CoG-101043998, DEEPCONTROL".

Declaration of interests. The authors report no conflict of interest.

Data availability statement. The data that support the findings of this study will be openly available on GitHub–KTH-Complex-fluids-group upon publication.

REFERENCES

- DUBIEF, Y., TERRAPON, V.E., WHITE, C.M., SHAQFEH, E.S.G., MOIN, P. & LELE, S.K. 2005 New answers on the interaction between polymers and vortices in turbulent flows. *Flow Turbul. Combust.* **74** (4), 311–329.
- DUBIEF, Y., WHITE, C.M., TERRAPON, V.E., SHAQFEH, E.S.G., MOIN, P. & LELE, S.K. 2004 On the coherent drag-reducing and turbulence-enhancing behaviour of polymers in wall flows. *J. Fluid Mech.* **514**, 271–280.
- FATTAL, R. & KUPFERMAN, R. 2004 Constitutive laws for the matrix-logarithm of the conformation tensor. *J. Non-Newtonian Fluid Mech.* **123** (2-3), 281–285.
- GUASTONI, L., GÜEMES, A., IANIRO, A., DISCETTI, S., SCHLATTER, P., AZIZPOUR, H. & VINUESA, R. 2021 Convolutional-network models to predict wall-bounded turbulence from wall quantities. *J. Fluid Mech.* **928**, A27.
- IZBASSAROV, D., ROSTI, M.E., BRANDT, L. & TAMMISOLA, O. 2021 Effect of finite weissenberg number on turbulent channel flows of an elastoviscoplastic fluid. *J. Fluid Mech.* **927**, A45.
- LE CLAINCHE, S., IZBASSAROV, D., ROSTI, M., BRANDT, L. & TAMMISOLA, O. 2020 Coherent structures in the turbulent channel flow of an elastoviscoplastic fluid. *J. Fluid Mech.* **888**, A5.
- NAGAMACHI, A. & TSUKAHARA, T. 2019 Predictability Study of Viscoelastic Turbulent Channel Flow Using Deep Learning. In *Fluids Eng. Div. Sum. Meet.*, p. V002T02A077. American Society of Mechanical Engineers.
- ROSTI, M.E., IZBASSAROV, D., TAMMISOLA, O., HORMOZI, S. & BRANDT, L. 2018 Turbulent channel flow of an elastoviscoplastic fluid. *J. Fluid Mech.* **853**, 488–514.
- VINUESA, R. 2024 Perspectives on predicting and controlling turbulent flows through deep learning. *Phys. Fluids* **36** (3).
- VINUESA, R., BRUNTON, S. L. & MCKEON, B. J. 2023 The transformative potential of machine learning for experiments in fluid mechanics. *Nat. Rev. Phys.* **5** (9), 536–545.
- VIRK, P.S. 1971 Drag reduction in rough pipes. *J. Fluid Mech.* **45** (2), 225–246.
- XI, L. 2019 Turbulent drag reduction by polymer additives: Fundamentals and recent advances. *Phys. Fluids* **31** (12).
- XI, L. & GRAHAM, M.D. 2010 Active and hibernating turbulence in minimal channel flow of Newtonian and polymeric fluids. *Phys. Rev. Lett.* **104** (21), 218301.
- XI, L. & GRAHAM, M.D. 2012 Intermittent dynamics of turbulence hibernation in Newtonian and viscoelastic minimal channel flows. *J. Fluid Mech.* **693**, 433–472.
- XU, Z.-Q.J., ZHANG, Y. & XIAO, Y. 2019 Training behavior of deep neural network in frequency domain. In *NeurIPS* (ed. T. Gedeon, K.W. Wong & M. Lee), pp. 264–274. Springer International Publishing.